PAPER

CrossMark
click for updates

Kinetics study of the Al–water reaction promoted by an ultrasonically prepared Al(OH)$_3$ suspension†

Gao-Heng Liang,[a] Wei-Zhuo Gai,[a] Zhen-Yan Deng,*[ab] Pingguang Xu[c] and Zhenxiang Cheng[bd]

The kinetics of the Al–water reaction promoted by an ultrasonically prepared Al(OH)$_3$ suspension is investigated. It is found that the induction time for the beginning of the Al–water reaction decreases and the reaction rate increases with increasing suspension concentration, volume, and temperature, because the Al–water reaction is exothermic. When the weight ratio of Al to water increases to 1 : 15, there is almost no induction time, and more than 80% of Al in the Al(OH)$_3$ suspension is consumed within 40 min, which is comparable to the behavior of Al in NaOH solution. A collision model based on Brownian motion is proposed to analyze the reaction process, which shows that the contact between Al and Al(OH)$_3$ particles and the reaction heat are two key factors that control the reaction progress.

1. Introduction

Hydrogen has a high calorific value, and its reaction by-product is environmentally benign, which makes it an ideal fuel for fuel cells. Storage and transportation of hydrogen remain a problem, however, due to its low boiling point ($-252\ ^\circ$C) and very poor compressibility. There has been a great deal of research to solve this problem. Hydrogen-generation materials are one of the choices, because they are reactive toward hydrolysis in water and generate hydrogen on site, which makes them suitable for portable applications. Al metal is a promising hydrogen-generation material due to its relatively low price, light atomic weight, and abundance ($\sim$8.1%) in the Earth's crust.[1,2] One kg of Al reacts with water to generate as much as 0.11 kg H$_2$, although, usually, there is a dense passive oxide film on the Al particle surface, inhibiting the reaction of Al with water.[3–5]

In the past few years, many methods have been developed to activate Al metal so that Al can directly react with water, *e.g.* using an alkaline solution,[6–14] alloying Al by doping with Ga, In, Bi, Sn, *etc.*,[15–23] mechanically milling Al metal with special oxides and soluble inorganic salts,[24–29] mixing Al with alkaline chemicals,[30–33] ceramic oxide modification, *etc.*[34–39] For the above methods, however, the pollution concerns about alkaline solutions, the high price of rare metals, and the need for complicated activation procedures have set back the prospects for Al–hydrogen technology in commercial applications.

Recently, a neutral Al(OH)$_3$ suspension was used to promote the Al–water reaction,[40–46] and no processing procedure was needed to activate the Al metal. Therefore, this is a relatively simple way to realize the Al–water reaction to generate hydrogen, although the Al–water reaction rate is slow if commercial Al(OH)$_3$ powder is used. Yang *et al.* prepared a high-activity Al(OH)$_3$ suspension by the reaction of Al with water using an ultrasonic procedure.[42] This high-activity Al(OH)$_3$ suspension considerably promotes the Al–water reaction and hydrogen generation. In this work, the Al–water reaction kinetics promoted by the ultrasonically prepared Al(OH)$_3$ suspension is investigated, with the results indicating that when the weight ratio of Al to water increases to a high value in practical application, the hydrogen-generation rate is fast and comparable to that of Al in NaOH solution, which could meet the practical requirement.

2. Experimental procedure

Two kinds of Al powders with the average sizes of 1.32 μm (99.9% purity, Henan Yuan Yang Aluminum Industry Co., China) and 7.29 μm (99.9% purity; High Purity Chemical Co., Tokyo, Japan) were used in the present study. The procedure to prepare Al(OH)$_3$ suspension by an ultrasonic method was given in a previous work,[42] where 1.32 μm Al powder was put into a beaker with deionized water, and then ultrasonically treated in an ultrasonic vessel (40 kHz, 150 W) at 40 °C for a certain time period ($\sim$4.5 h) so that the Al powder could completely react with water.

[a]Energy Materials & Physics Group, Department of Physics, Shanghai University, Shanghai 200444, China. E-mail: zydeng@shu.edu.cn; Fax: +86-21-66134208; Tel: +86-21-66134334

[b]Shanghai Key Laboratory of High Temperature Superconductors, Shanghai University, Shanghai 200444, China

[c]Japan Atomic Energy Agency, Tokai, Ibaraki 319-1195, Japan

[d]Institute for Superconducting and Electronic Materials, University of Wollongong, North Wollongong, Wollongong, NSW 2500, Australia

† Electronic supplementary information (ESI) available. See DOI: 10.1039/c6ra01627h

The Al–water reaction tests in the above ultrasonically prepared $Al(OH)_3$ suspension were carried out in a closed glass reactor with a volume of ~1300 ml, under which a thermostatically controlled water bath was placed to control the reaction temperature (if not specially mentioned).[47] The real temperature in the $Al(OH)_3$ suspension was measured by a thermometer inside the reactor. 7.29 μm Al powder was used in all the reaction tests, in which the Al powder was suspended in $Al(OH)_3$ suspension and no agitation was used. As the reaction of Al with water produces only H_2, the amount of generated H_2 was used to characterize the progress of the reaction of Al with water. The hydrogen evolution is determined by the gas pressure in the reactor using the ideal-gas equation:

$$\alpha_s = \frac{(P - P_{initial})(V_{reactor} - V_{H_2O} - V_{Al})}{n_0 RT} \quad (1)$$

where α_s is the hydrogen yield; P and $P_{initial}$ are the total gas pressure and the initial gas pressure in the reactor, respectively (the initial gas pressure is 1 bar); $V_{reactor}$, V_{H_2O}, and V_{Al} are the volumes of the reactor, water, and Al powder, respectively; and n_0 is the theoretical number of hydrogen moles obtained by reacting all of the Al metal. At least two identical tests were carried out to test the reproducibility of each hydrogen-generation curve. Scanning electron microscopy (SEM) was used to observe the morphologies of the pure Al powders and the $Al(OH)_3$ obtained by filtering and drying the $Al(OH)_3$ suspension.

3. Results

Fig. 1 shows the morphologies of the pure Al powders and the $Al(OH)_3$ particles obtained from the $Al(OH)_3$ suspension.

Basically, Al particles are spherical, and there is a particle size distribution, but some of the Al particles in the 7.29 μm Al powder are not exactly spherical. The $Al(OH)_3$ particles are sheet- and flower-like, and their sizes are on the order of 150 nm, so this size will be used in the following model calculations. The phase composition of $Al(OH)_3$ particles has been identified in Fig. 11 of ref. 42.

Fig. 2 shows H_2 evolution by the addition of 7.29 μm Al powder into deionized water (250 ml) or $Al(OH)_3$ suspensions with different volumes at 25 °C, where 1.0 g of Al powder is added into water or suspension in each test and the solid volume ratio of Al to $Al(OH)_3$ in the suspension is always 9 : 1.
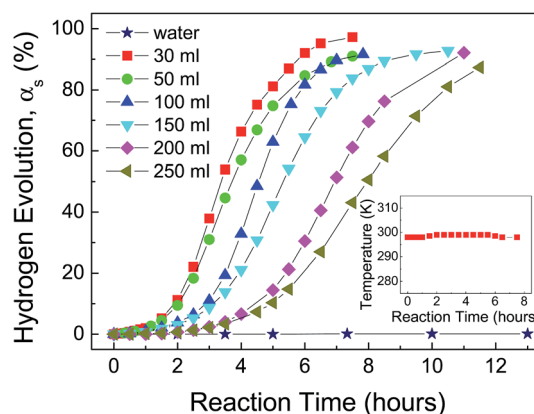

Fig. 2 H_2 evolution by the addition of 7.29 μm Al powder into deionized water (250 ml) or $Al(OH)_3$ suspensions with different volumes at 25 °C, where 1.0 g of Al powder is used in each test and the solid volume ratio of Al to $Al(OH)_3$ in the suspension is always 9 : 1. The inset shows the variation of temperature with time for the Al–water reaction in 30 ml $Al(OH)_3$ suspension.
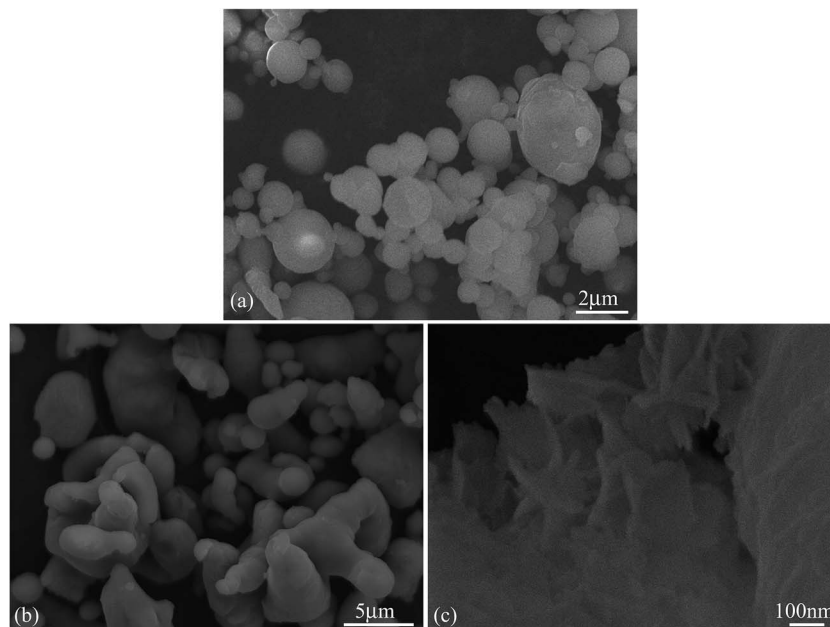

Fig. 1 SEM micrographs of pure Al powders with the average particle sizes of 1.32 μm (a) and 7.29 μm (b), and $Al(OH)_3$ powder prepared by the reaction of 1.32 μm Al powder with water using an ultrasonic procedure (c).

The induction time for the Al–water reaction in deionized water is long (>50 h, details not shown), however, it decreases to ~3 h when an high-activity $Al(OH)_3$ suspension with the same volume is used. It can be seen that when the weight ratio of Al to water in the suspension increases from 1 : 250 (250 ml water) to 1 : 30 (30 ml water), the induction time decreases from ~3 h to ~1 h, indicating that increasing the $Al(OH)_3$ concentration in the suspension decreases the induction time, because the amount of $Al(OH)_3$ in all the suspensions is the same. The inset in Fig. 2 shows that there is a small temperature rise during the reaction in the 30 ml suspension, even though a thermostatically controlled water bath is used, indicating that the reaction heat (426.5 kJ mol Al^{-1}) cannot diffuse away within a limited time.

Fig. 3 shows H_2 evolution by the addition of 7.29 μm Al powder into $Al(OH)_3$ suspensions with a solid volume ratio of Al to $Al(OH)_3$ in the suspension that is always 8 : 2, where the other parameters are the same as those in Fig. 2. Compared with the results in Fig. 2, it is clear that the induction time decreases and the reaction rate increases with increasing $Al(OH)_3$ concentration in suspensions with the same volume. In Fig. 3, when the weight ratio of Al to water in the suspension increases from 1 : 250 (250 ml water) to 1 : 30 (30 ml water), the induction time decreases from ~2 h to ~0.5 h. Furthermore, the temperature rise during the reaction in the 30 ml suspension in Fig. 3 is higher than that in Fig. 2, indicating that more reaction heat doesn't diffuse away due to the faster reaction rate.

Fig. 4 shows H_2 evolution by the addition of 7.29 μm Al powder into 30 ml of $Al(OH)_3$ suspension at different temperatures, where the weight ratio of Al to water in the suspension is 1 : 30. It can be seen that the induction time decreases and the reaction rate increases with increasing temperature. The induction time for a solid volume ratio 8 : 2 of Al to $Al(OH)_3$ in the suspension is shorter and its reaction rate is faster than those for a solid volume ratio 9 : 1. For the suspension with the solid volume ratio 8 : 2 of Al to $Al(OH)_3$, when the temperature increases to 35 °C (308 K), there is no reaction induction time,
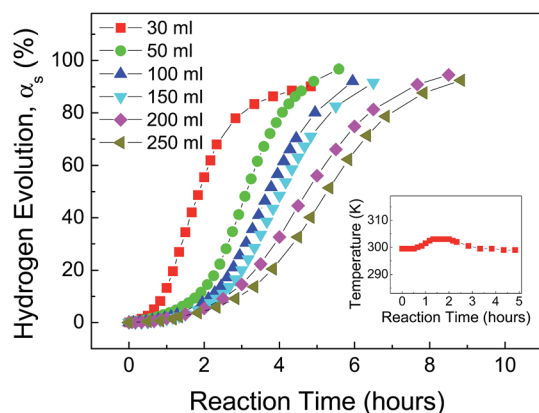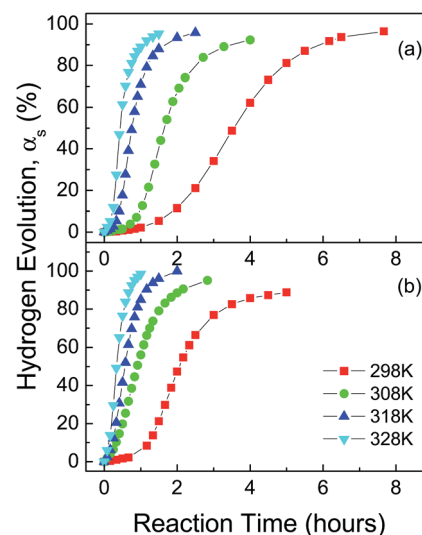

Fig. 4 H_2 evolution by the addition of 7.29 μm Al powder into 30 ml of $Al(OH)_3$ suspension at different temperatures, where 1.0 g of Al powder is used in each test and the solid volume ratio of Al to $Al(OH)_3$ in the suspension is always (a) 9 : 1 and (b) 8 : 2, respectively.

and >90% of the Al metal is consumed within 2.5 h. When the temperature is 55 °C (328 K), >90% of the Al metal is consumed within 1 h for both of the above suspensions. This indicates that temperature is an important factor affecting the induction time and reaction rate.

If no thermostatically controlled water bath is used, the heat generated by the Al–water reaction will diffuse more slowly, because the thermal conductivity of air (0.023 W m^{-1} K^{-1}) is much lower than that of water (0.6 W m^{-1} K^{-1}), which is close to the situation in practical application. In this case, the temperature of the suspension will increase rapidly with the progress of the reaction. Fig. 5 shows the H_2 evolution and variation of water temperature by the addition of 7.29 μm Al powder into the $Al(OH)_3$ suspension at an initial temperature of 25 °C without thermostatic control of the water bath, where the weight ratio of Al to water is always 1 : 30 and the solid volume ratio of Al to $Al(OH)_3$ in the suspensions is 8 : 2. (This means that the amount of Al powder increases linearly with increasing suspension volume.) It can be seen that the reaction rate and water temperature rise increase rapidly with increasing suspension volume. This is because with the increase in suspension volume, more Al metal joins the reaction, and more reaction heat is released as the reaction progresses, so that the water temperature increases more rapidly (Fig. 5(b)), leading to an increase in the Al–water reaction rate (Fig. 5(a)). When the suspension volume is 250 ml, the highest suspension temperature is ~92.5 °C, and >90% of metal Al is consumed within 1 h.

As the weight ratio of Al to water in the ideal reaction equation is 1 : 2,[1] in practical application, this ratio in the suspension should be above 1 : 15. Fig. 6 shows H_2 evolution and variation of water temperature by the addition of 7.29 μm Al powder into $Al(OH)_3$ suspensions with different Al to water ratios, where the suspension volume is 50 ml and the solid

Fig. 3 H_2 evolution by the addition of 7.29 μm Al powder into $Al(OH)_3$ suspensions with different volumes at 25 °C, where 1.0 g of Al powder is used in each test and the solid volume ratio of Al to $Al(OH)_3$ in the suspension is always 8 : 2. The inset shows the variation of temperature with time for the Al–water reaction in 30 ml $Al(OH)_3$ suspension.

**Fig. 5** (a) H_2 evolution and (b) variation of water temperature for the Al–water reaction by the addition of 7.29 μm Al powder into Al(OH)$_3$ suspensions with different volumes, where the initial temperature in the suspensions is 25 °C, the weight ratio of Al to water is always 1 : 30 and the solid volume ratio of Al to Al(OH)$_3$ in the suspension is 8 : 2. No thermostat is used in this experiment.

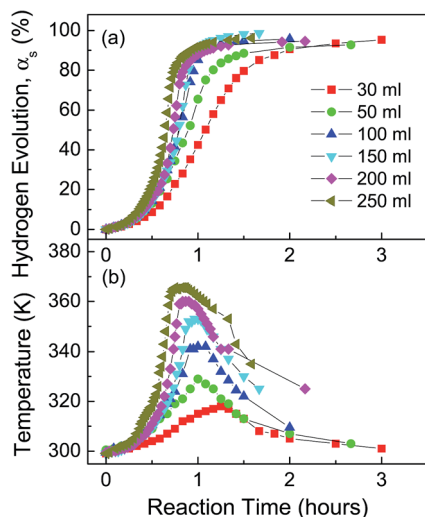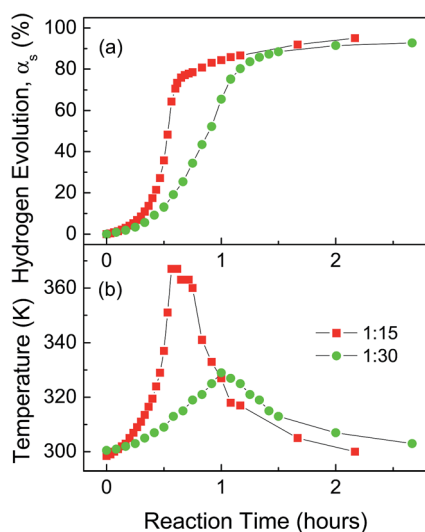**Fig. 6** (a) H_2 evolution and (b) variation of water temperature for the Al–water reaction by the addition of 7.29 μm Al powder into 50 ml of Al(OH)$_3$ suspension with different Al to water weight ratios, where the initial temperature in the suspensions is 25 °C and the solid volume ratio of Al to Al(OH)$_3$ in the suspension is 8 : 2. No thermostat is used in this experiment.

volume ratio of Al to Al(OH)$_3$ in suspension is always 8 : 2. It can been seen that when the weight ratio of Al to water in the suspension increases to 1 : 15, the highest suspension temperature is ~94 °C, and >80% of the Al metal in the Al(OH)$_3$ suspension is consumed within 40 min. This reaction rate is comparable to that of Al powder in NaOH solution and could meet the practical requirement for portable applications.[9]

4. Model analyses

4.1 Induction time

A previous study showed that the induction time required before the beginning of the Al–water reaction originates from the hydration of the passive oxide film on the Al surface.[3] When the hydrated front meets the metal beneath the Al surface, the water molecules react with the Al metal and generate hydrogen. H_2 molecules accumulate to form small H_2 bubbles at the Al : Al$_2$O$_3$ interface. When the reaction gas pressure in the H_2 bubbles exceeds the critical gas pressure that the hydrated oxide film can sustain (Fig. 2 in ref. 3), the film on the Al particle surface breaks. Then, the Al surface on the inside comes in direct contact with the water on the outside, and the beginning of the Al–water reaction is observed. The induction time is the time period that extends from putting the Al particles into water to the breaking of the Al surface oxide film.

It was confirmed that Al(OH)$_3$ particles can act as a catalyst to assist the reaction of Al with water,[39–42] because Al(OH)$_3$ can dissociate H_2O molecules into ions, which can promote the hydration of the passive oxide film on the Al surface when Al(OH)$_3$ particles come into contact with Al particles in water, leading to a shorter induction time for the Al–water reaction. Therefore, the contact area between the Al(OH)$_3$ and Al particles is an important factor that affects the catalytic performance towards the Al–water reaction.

When no agitation is used, the movement of small particles (usually <10 μm) in liquid observes the rule of Brownian motion, which is caused by collisions with molecules of the surrounding medium.[48,49] The speed of Brownian particles in solution follows the Maxwell–Boltzmann rate distribution:

$$f(v) = 4\pi \left(\frac{m^*}{2\pi kT}\right)^{3/2} \exp\left(-\frac{m^* v^2}{2kT}\right) v^2 \tag{2a}$$

where

$$m^* = m + \frac{1}{2} m_f \quad \text{with} \quad m_f = \frac{4}{3}\pi r^3 \rho_L \tag{2b}$$

is the effective mass of the Brownian particle in liquid, which is the sum of the particle mass and half of the mass of the displaced fluid (m_f).[49] Here, a spherical particle with a radius of r is assumed, and the liquid density is ρ_L. The average speed of Brownian particles in solution can be calculated as[50]

$$\bar{v} = \int_0^\infty v f(v) \mathrm{d}v = \sqrt{\frac{8kT}{\pi m^*}}. \tag{3}$$

If two kind of particles with different masses m_1 and m_2 move in the same liquid, their relative average speed can be obtained by vector calculation[50]

$$\bar{v}_{12} = \sqrt{\frac{8kT}{\pi \mu}} \tag{4a}$$

where

$$\mu = \frac{m_1^* m_2^*}{m_1^* + m_2^*} \tag{4b}$$

is the reduced mass, and m_1^* and m_2^* are the effective masses of the two kinds of particles in the liquid. If Al and Al(OH)$_3$ particles are assumed to be spherical with radii of r_1 and r_2, respectively, the average collision frequency per unit time between one Al particle and the Al(OH)$_3$ particles in the water can be written as

$$\overline{Z}_1 = \frac{N_2}{V}\pi(r_1 + r_2)^2 \overline{v}_{12} = \frac{N_2}{V}(r_1 + r_2)^2 \sqrt{\frac{8\pi kT}{\mu}} \quad (5)$$

where V is the water volume and N_2 is the total number of Al(OH)$_3$ particles. N_2 is equal to the Al(OH)$_3$ mass in suspension divided by one Al(OH)$_3$ particle mass.

Previous work[3] indicated that the induction time for the Al–water reaction includes three parts

$$t_0 = t_i + t_s + t_e \quad (6)$$

where t_i is the hydration time of the native oxide film, t_s is the time from the beginning of H$_2$ generation at the Al : Al$_2$O$_3$ interface to the H diffusion saturation in bulk Al, and t_e is the time interval from the H diffusion saturation in bulk Al to the time that the gas pressure in H$_2$ bubbles at the Al : Al$_2$O$_3$ interface reaches the critical value. As Al(OH)$_3$ particles promote the hydration of the Al surface oxide film, the hydration rate, v_h, should be proportional to the contact area between the Al and the Al(OH)$_3$ particles

$$v_h = \frac{k_1 \overline{Z}_1}{4\pi r_1^2} S \quad (7a)$$

with

$$k_1 = k_{10} \exp\left(-\frac{E_1}{RT}\right) \quad (7b)$$

the rate constant for the catalytic hydration reaction by Al(OH)$_3$, where k_{10} is a constant and E_1 is the activation energy for the hydration reaction. The maximum contact area between one Al particle and an Al(OH)$_3$ particle during an elastic collision is (see the ESI†)

$$S = 2r_2 \sqrt[3]{\frac{3\pi kT}{E}} \quad (8)$$

where it is assumed that Al and Al(OH)$_3$ have the same Young's modulus (E). The hydration rate can be obtained by inserting eqn (5) and (8) into eqn (7)

$$v_h = 2k_{10}\frac{N_2}{V}\left(1 + \frac{r_2}{r_1}\right)^2 r_2 \sqrt[6]{\frac{9k^5 T^5}{8\pi\mu^3 E^2}}\exp\left(-\frac{E_1}{RT}\right). \quad (9)$$

If it is assumed that the oxide film thickness of Al particles with different radii is the same (h),[3] the hydration time of the native oxide film can be written as

$$t_i = \frac{h}{v_h} = \frac{c_1}{\frac{N_2}{V}\left(1 + \frac{r_2}{r_1}\right)^2 r_2 \sqrt[6]{\frac{T^5}{\mu^3}}}\exp\left(\frac{E_1}{RT}\right) \quad (10a)$$

with

$$c_1 = \frac{h}{2k_{10}\sqrt[6]{\frac{9k^5}{8\pi E^2}}}. \quad (10b)$$

where v_h is the movement velocity of the hydration front of the Al surface oxide film, which represents the transportation speed of water molecules moving to the Al : Al$_2$O$_3$ interface. As both the H diffusion saturation and the critical gas pressure in H$_2$ bubbles at the Al : Al$_2$O$_3$ interface are related to the Al particle volume,[3,47] if the water molecule transportation is the rate-controlling step, then

$$t_s + t_e = \frac{k_2 r_1}{v_h} = \frac{c_2 r_1}{\frac{N_2}{V}\left(1 + \frac{r_2}{r_1}\right)^2 r_2 \sqrt[6]{\frac{T^5}{\mu^3}}}\exp\left(\frac{E_1}{RT}\right) \quad (11a)$$
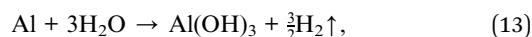
with

$$c_2 = \frac{k_2}{2k_{10}\sqrt[6]{\frac{9k^5}{8\pi E^2}}} \quad (11b)$$

where k_2 is a constant. The total induction time is as follows:

$$t_0 = t_i + t_s + t_e = \frac{(c_1 + c_2 r_1)}{\frac{N_2}{V}\left(1 + \frac{r_2}{r_1}\right)^2 r_2 \sqrt[6]{\frac{T^5}{\mu^3}}}\exp\left(\frac{E_1}{RT}\right). \quad (12)$$

4.2 Reaction temperature

The reaction equation of Al with water can be written as[1,41]

$$Al + 3H_2O \rightarrow Al(OH)_3 + \tfrac{3}{2}H_2\uparrow, \quad (13)$$

$$\Delta H_{298}^0 = -426.5 \text{ kJ mol}^{-1}$$

which is an exothermic reaction. Therefore, the temperature of the suspension will increase as the reaction progresses

$$T = T_0 + \frac{\Delta Q - \Delta Q_s}{m_w c_w} \quad (14)$$

where T_0 is the initial temperature, and m_w and c_w are the water mass and specific heat, respectively. The total released reaction heat is

$$\Delta Q = -\alpha_s M_{Al}\Delta H_{298}^0 \quad (15)$$

where α_s is the reaction ratio for the Al metal and M_{Al} is the number of Al moles. The heat diffused to the outside during the reaction is

$$\Delta Q_s = k_s S_v t \frac{T - T_0}{2} = k_s\left(36\pi V^2\right)^{1/3} t\frac{T - T_0}{2} \quad (16)$$

where k_s is the heat diffusivity per unit time and area, t is the reaction time (excluding the induction time), and S_v is the surface area of the suspension. Here, as an approximation, the shape of the suspension is viewed as a sphere, and a linear

temperature rise is assumed. The suspension temperature can be obtained by inserting eqn (15) and (16) into eqn (14)

$$T = T_0 - \frac{\alpha_s M_{Al} \Delta H_{298}^0}{m_w c_w + \frac{k_s (36\pi V^2)^{1/3} t}{2}} \quad (17)$$

4.3 Hydrogen evolution

The Al–water reaction is a solid–liquid heterogeneous system, and its reaction dynamics can be described by the shrinking core model.[47] It was confirmed that at the initial stage (excluding the induction time), the surface chemical reaction is the rate-controlling step, and its rate equation can be written[47]

$$1 - (1 - \alpha)^{1/3} = k_2 t \quad (18a)$$

with

$$k_2 = k_{20} \exp\left(-\frac{E_2}{RT}\right) \quad (18b)$$

the rate constant for the Al–water reaction, where α is the hydrogen yield of the considered Al particle, k_{20} is a constant and E_2 is the activation energy. In fact, the activation energy, E_2, is a function of the Al particle size[47] and can be described by

$$E_2 = a + br_1 \quad (19)$$

where a and b are the constants, which can be obtained by fitting the experimental results in Fig. 11 of ref. 47. From eqn (18), the hydrogen yield of one Al particle can be obtained

$$\alpha = 1 - (1 - k_2 t)^3 = 1 - \left[1 - k_{20} t \exp\left(-\frac{E_2}{RT}\right)\right]^3 \quad (20)$$

In the real Al powder, there is a particle size distribution, which can be described by a log-normal function[51]

$$f(r_1) = \frac{A}{r_1 \sigma \sqrt{2\pi}} \exp\left[-\frac{(\ln r_1 - \mu)^2}{2\sigma^2}\right] \quad (21)$$

where A is a constant, σ is the standard deviation, and $\mu = \ln r_v$ with r_v the average radius. As the induction time is a function of the Al particle size, the dependence of total hydrogen yield on time for Al powder can be written

$$\alpha_s = \frac{\int_0^\infty \theta(t - t_0)\alpha(t - t_0)f(r_1)r_1^3 dr_1}{\int_0^\infty f(r_1)r_1^3 dr_1}$$

$$= \frac{\int_0^\infty \theta(t - t_0)\left\{1 - \left[1 - k_{20}(t - t_0)\exp\left(-\frac{E_2}{RT}\right)\right]^3\right\}f(r_1)r_1^3 dr_1}{\int_0^\infty f(r_1)r_1^3 dr_1}$$

$$\qquad\qquad\qquad\qquad\qquad\qquad\qquad\qquad\qquad (22)$$

where

$$\theta(t - t_0) = \begin{cases} 1 & t > t_0 \\ 0 & t < t_0 \end{cases} \quad (23)$$

is a step function. Eqn (22) can be calculated self-consistently by combining it with eqn (12) and (17), using a Fortran program on a workstation.

4.4 Numerical calculation

Before the numerical calculations, the parameters in the above equations need to be determined. The effective masses of the Al and $Al(OH)_3$ particles can be calculated by eqn (2b), and their masses are

$$m_1 = \frac{4}{3}\pi r_1^3 \rho_{Al} \quad \text{and} \quad m_2 = \frac{4}{3}\pi r_2^3 \rho_{Al(OH)_3}$$

where ρ_{Al} and $\rho_{Al(OH)_3}$ are the densities of the Al and $Al(OH)_3$ particles, respectively. In the numerical calculations, 7.29 μm Al powder is considered, and the parameters A, σ, and r_v are obtained by fitting the 7.29 μm Al particle size distribution (Fig. 12(a) in ref. 47) with eqn (21). In order to determine the parameters in eqn (12), (1.32) μm Al powder was also used for hydrogen-generation testing, where 1.0 g of Al powder was added into 250 ml $Al(OH)_3$ suspension with a solid volume ratio 9 : 1 of Al to $Al(OH)_3$ at 25 °C. The induction time for 1.32 μm Al powder is 0.91 h, so by combining this result with the induction time (2.5 h) of 7.29 μm Al powder under the same conditions (Fig. 2), we can obtain the ratio of c_1 to c_2, where the average size is viewed as the size of all the Al particles. The final values of c_1, c_2, and E_1 can be obtained by fitting the induction time at different temperatures in Fig. 4(a) with eqn (12). As the temperature rise for the Al–water reaction in 30 ml $Al(OH)_3$ suspension in Fig. 5(b) is approximately linear from the beginning of the reaction to the time of the highest temperature point, we used eqn (17) to fit the data in 30 ml $Al(OH)_3$ suspension for this time interval and obtained the heat diffusivity k_s. The constant k_{20} in eqn (18b) can be obtained from the rate constant k_2 for the Al–water reaction using 7.29 μm Al powder in 250 ml deionized water at 40 °C (Fig. 10 in ref. 47). The fitting software used in this work is OriginPro 8.0, the physical and fitting parameters are listed in Tables 1 and 2, respectively.

Fig. 7 shows the theoretical dependence of the induction time for the Al–water reaction on the Al particle size at different temperatures in 250 ml $Al(OH)_3$ suspension, where 1 g of Al powder was used in each test. It can be seen that the induction time increases with increasing Al particle size and decreases with increasing temperature and $Al(OH)_3$ content in the suspension, which is consistent with the experimental results in Fig. 2–4. Fig. 8 shows the dependence of induction time on
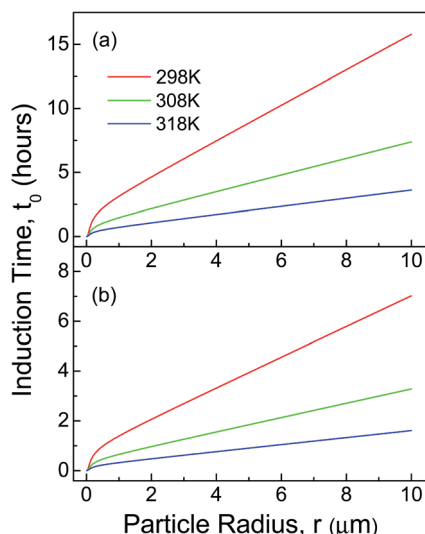
Table 1 The physical parameters used in the model calculation

Parameter	Value
ρ_L	1.0 g cm^{-3}
ρ_{Al}	2.70 g cm^{-3}
$\rho_{Al(OH)_3}$	2.42 g cm^{-3}
c_w	4.178 J g^{-1} K^{-1}
r_2	150 nm

Table 2 The parameters obtained by fitting the related equations with the experimental data

Parameter	Value
A	0.17656 μm
σ	0.63134
r_v	1.4688 μm
c_1	4.004×10^{-3} hour $K^{5/6}$ μm^{-2} g$^{-1/2}$
c_2	2.472×10^{-3} hour $K^{5/6}$ μm^{-3} g$^{-1/2}$
E_1	55.89 kJ mol^{-1}
k_s	15.23 J K^{-1} cm^{-2} hour^{-1}
a	64.98 kJ mol^{-1}
b	0.8635 kJ mol^{-1} μm^{-1}
k_{20}	3.759×10^{10} hour^{-1}

Fig. 8 Dependence of induction time for the Al–water reaction on suspension volume at different temperatures, where the Al particle size is 7.29 μm, 1 g of Al is used in each test, and the solid volume ratio of Al to Al(OH)$_3$ in the suspension is (a) 9 : 1 and (b) 8 : 2, respectively.

Fig. 7 Dependence of induction time for the Al–water reaction on Al particle size at different temperatures in 250 ml Al(OH)$_3$ suspension, where 1 g of Al is used in each test and the solid volume ratio of Al to Al(OH)$_3$ in the suspension is (a) 9 : 1 and (b) 8 : 2, respectively.

Fig. 9 Variation of (a) hydrogen yield and (b) water temperature with time for the Al–water reaction in Al(OH)$_3$ suspensions with different volumes, where the initial temperature is 25 °C, 1 g of 7.29 μm Al powder with a particle size distribution is used in each test, and the solid volume ratio of Al to Al(OH)$_3$ in the suspension is 9 : 1.

water volume at different temperatures, where 1 g of Al powder was used in each test. It can be seen that when the Al content in the suspension is a constant, the induction time increases with increasing water volume and decreases with increasing temperature and Al(OH)$_3$ content, which is also in agreement with the experimental results in Fig. 2–4.

Fig. 9 and 10 show the hydrogen evolution and water temperature for the Al–water reaction in Al(OH)$_3$ suspensions with different volumes, where 1 g of 7.29 μm Al powder with a particle size distribution is used in each test. It can be seen that when the weight of Al powder in the suspension is a constant, the induction time increases and the hydrogen-generation rate decreases with increasing water volume, which is consistent with the experimental results in Fig. 2 and 3. Furthermore, the induction time decreases and the hydrogen-generation rate increases with increasing Al(OH)$_3$ content in the suspension, which is also in agreement with the experimental results in Fig. 2 and 3. At the same time, the water
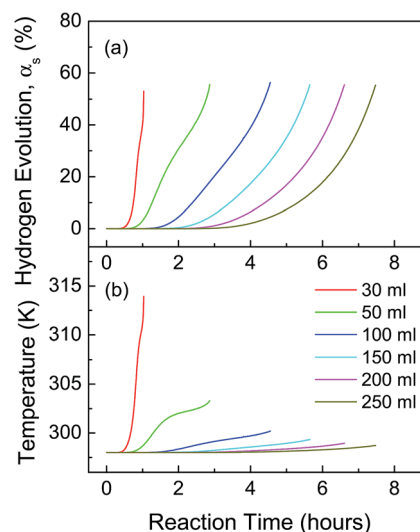
temperature rise decreases with increasing water volume, but the theoretical value in 30 ml Al(OH)$_3$ suspension in Fig. 9 and 10 is much higher than the experimental temperature rise in Fig. 2 and 3. This is because in the practical experiment, a thermostatically controlled water bath is used to control the temperature, while no thermostat is considered in the theoretical calculation.

Fig. 11 and 12 show the hydrogen evolution and water temperature for the Al–water reaction in 30 ml of Al(OH)$_3$ suspension for different initial temperatures, where 1 g of 7.29
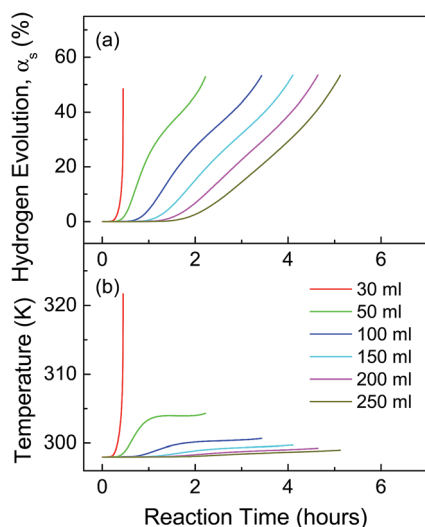
Fig. 10 Variation of (a) hydrogen yield and (b) water temperature with time for the Al–water reaction in $Al(OH)_3$ suspensions with different volumes, where the initial temperature is 25 °C, 1 g of 7.29 µm Al powder with a particle size distribution is used in each test, and the solid volume ratio of Al to $Al(OH)_3$ in the suspension is 8 : 2.

Fig. 12 Variation of (a) hydrogen yield and (b) water temperature with time for the Al–water reaction in 30 ml of $Al(OH)_3$ suspension at different initial temperatures, where 1 g of 7.29 µm Al powder with a particle size distribution is used in each test and the solid volume ratio of Al to $Al(OH)_3$ in the suspension is 8 : 2.

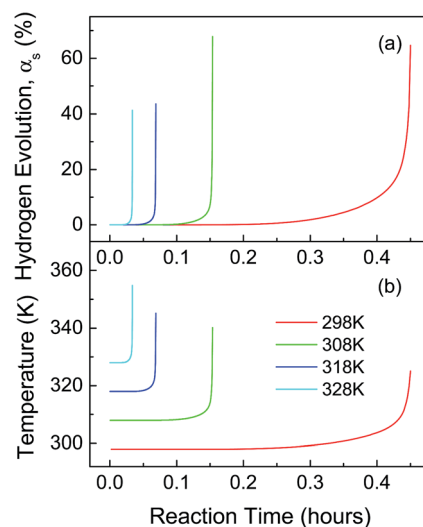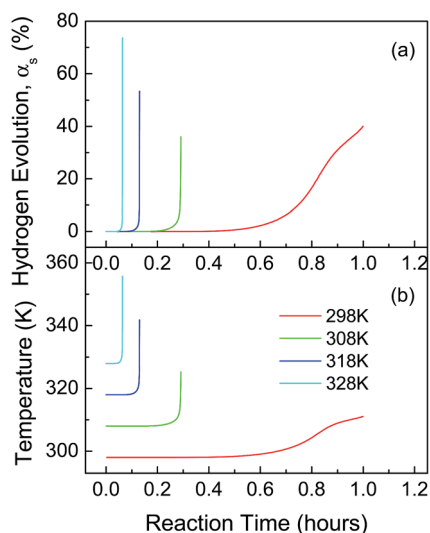**Fig. 11** Variation of (a) hydrogen yield and (b) water temperature with time for the Al–water reaction in 30 ml of $Al(OH)_3$ suspension at different initial temperatures, where 1 g of 7.29 µm Al powder with a particle size distribution is used in each test and the solid volume ratio of Al to $Al(OH)_3$ in the suspension is 9 : 1.

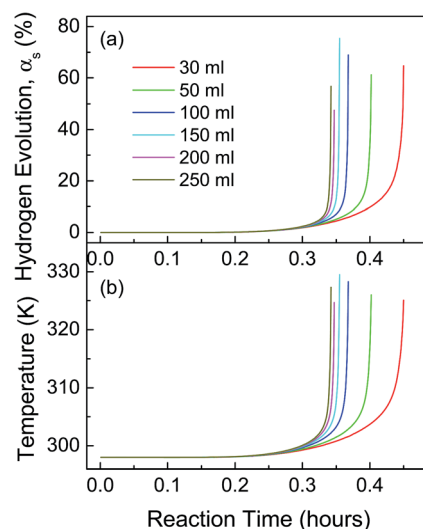**Fig. 13** Variation of (a) hydrogen yield and (b) water temperature with time for the Al–water reaction in $Al(OH)_3$ suspensions with different volumes using 7.29 µm Al powder with a particle size distribution, where the initial temperature of the suspensions is 25 °C, the weight ratio of Al to water is always 1 : 30 and the solid volume ratio of Al to $Al(OH)_3$ in the suspension is 8 : 2.

µm Al powder is used in each test. It can be seen that the induction time decreases and the hydrogen-generation rate increases with increasing initial temperature and increasing $Al(OH)_3$ content in the suspension, which is consistent with the experimental results in Fig. 4. Furthermore, the water temperature rise increases with increasing initial temperature and increasing $Al(OH)_3$ content.

Fig. 13 shows the hydrogen evolution and water temperature for the Al–water reaction in $Al(OH)_3$ suspensions with different volumes using 7.29 µm Al powder, where the weight ratio of Al

to water is always 1 : 30 and the solid volume ratio of Al to $Al(OH)_3$ is 8 : 2. It can be seen that the induction time decreases, and the hydrogen-generation rate and the rate at which the water temperature rises increase with increasing suspension volume. These results are consistent with the experimental results in Fig. 5.

It should be noted that the theoretical results in Fig. 7–13 are in qualitative agreement with the experimental results, indicating that the theoretical analyses reveal the basic physical

mechanisms in the Al–water reaction promoted by the $Al(OH)_3$ suspension, although there is a difference in the quantitative comparisons between the theoretical calculations and the experimental results. This is because the rate eqn (18) describing the Al–water reaction is only suitable for the initial stage of the reaction. After the initial stage, the mass transfer in the by-product layer is the rate-controlling step, and in this case, the rate eqn (18) is inapplicable.[47] For Al powder with a particle size distribution, the small Al particles will start to react at an earlier time than the large Al particles due to their different induction times, so it is possible that the small Al particles have reacted away when the large Al particles start to react. Therefore, the model analyses are only suitable for the initial stage of the Al–water reaction.

In fact, eqn (12) indicates that the induction time for the Al–water reaction is proportional to the Al radius and inversely proportional to the $Al(OH)_3$ concentration (N_2/V) and temperature, because an Al particle with a larger radius takes a longer time to reach H diffusion saturation in the bulk Al and the critical gas pressure in the H_2 bubbles at the $Al : Al_2O_3$ interface (eqn (11a)). Increasing the $Al(OH)_3$ concentration will increase the collision frequency between the Al and $Al(OH)_3$ particles (eqn (5)), leading to an increase in their contact area. Moreover, increasing the temperature will increase the hydration reaction rate of the Al surface oxide film (eqn (7b)). This is why the induction time increases with increasing water volume when the $Al(OH)_3$ content is fixed, as shown in Fig. 3 and 4, and increasing the temperature decreases the induction time (Fig. 4). Eqn (17) indicates that the temperature rise during the Al–water reaction is proportional to the number of Al moles, because more heat is released when more Al joins the reaction. At the same time, the Al–water reaction rate is proportional to the temperature (eqn (18b)). As the Al powder has a particle size distribution, with the smaller particles reacting first, the induction time decreases, and the hydrogen-generation rate increases with increasing Al content, as shown in Fig. 5. Our results imply that it is possible for the Al–water reaction rate to reach the practical requirement for portable application if a higher $Al(OH)_3$ concentration and a suitable Al content are chosen.

5. Conclusions

In this work, the effects of kinetic factors on the Al–water reaction promoted by an ultrasonically prepared $Al(OH)_3$ suspension were investigated. It was found that the induction time for the Al–water reaction increases and the hydrogen-generation rate decreases with increasing water volume when the solid Al and $Al(OH)_3$ contents are fixed, because the $Al(OH)_3$ concentration in the suspension decreases. The induction time decreases, and the hydrogen-generation rate increases with increasing suspension volume when the ratio of Al to water and the $Al(OH)_3$ concentration are fixed, because more Al joins the reaction and produces more heat, leading to a faster and higher temperature rise. A model analysis has been conducted based on Brownian motion, which shows that the contact area between the Al and $Al(OH)_3$ particles and the reaction heat are

two important factors that affect the progress of the reaction. The theoretical calculations are in qualitative agreement with the experimental results.

References

1 Z. Y. Deng, J. M. F. Ferreira and Y. Sakka, *J. Am. Ceram. Soc.*, 2008, **91**, 3825–3834.
2 X. N. Huang, T. Gao, X. L. Pan, D. Wei, C. J. Lv, L. S. Qin and Y. X. Huang, *J. Power Sources*, 2013, **229**, 133–140.
3 Z. Y. Deng, J. M. F. Ferreira, Y. Tanaka and J. H. Ye, *J. Am. Ceram. Soc.*, 2007, **90**, 1521–1526.
4 W. Z. Gai and Z. Y. Deng, *Int. J. Hydrogen Energy*, 2014, **39**, 13491–13497.
5 Y. Yavor, S. Goroshin, J. M. Bergthorson and D. L. Frost, *Int. J. Hydrogen Energy*, 2015, **40**, 1026–1036.
6 D. Belitskus, *J. Electrochem. Soc.*, 1970, **117**, 1097–1099.
7 L. Soler, J. Macanas, M. Munoz and J. Casado, *Int. J. Hydrogen Energy*, 2007, **32**, 4702–4710.
8 L. Soler, A. M. Candela, J. Macanas, M. Munoz and J. Casado, *J. Power Sources*, 2009, **192**, 21–26.
9 C. R. Jung, A. Kundu, B. Ku, J. H. Gil, H. R. Lee and J. H. Jang, *J. Power Sources*, 2008, **175**, 490–494.
10 E. D. Wang, P. F. Shi, C. Y. Du and X. R. Wang, *J. Power Sources*, 2008, **181**, 144–148.
11 T. Hiraki and T. Akiyama, *Int. J. Hydrogen Energy*, 2009, **34**, 153–161.
12 H. B. Dai, G. L. Ma, H. J. Xia and P. Wang, *Energy Environ. Sci.*, 2011, **4**, 2206–2212.
13 M. K. Yu, M. J. Kim, B. Y. Yoon, S. K. Oh, D. H. Nam and H. S. Kwon, *Int. J. Hydrogen Energy*, 2014, **39**, 19416–19423.
14 G. D. Yao, X. Zeng, Y. J. Jin, H. Zhong, J. Duo and F. M. Jin, *Int. J. Hydrogen Energy*, 2015, **40**, 14284–14289.
15 O. V. Kravchenko, K. N. Semenenko, B. M. Bulychev and K. B. Kalmykov, *J. Alloys Compd.*, 2005, **397**, 58–62.
16 M. Q. Fan, F. Xu and L. X. Sun, *Int. J. Hydrogen Energy*, 2007, **32**, 2809–2815.
17 V. Rosenband and A. Gany, *Int. J. Hydrogen Energy*, 2010, **35**, 10898–10904.
18 W. Wang, D. M. Chen and K. Yang, *Int. J. Hydrogen Energy*, 2010, **35**, 12011–12019.
19 J. T. Ziebarth, J. M. Woodall, R. A. Kramer and G. Choi, *Int. J. Hydrogen Energy*, 2011, **36**, 5271–5279.
20 X. Y. Chen, Z. W. Zhao, X. H. Liu, M. M. Hao, A. L. Chen and Z. Y. Tang, *J. Power Sources*, 2014, **254**, 345–352.
21 S. Elitzur, V. Rosenband and A. Gany, *Int. J. Hydrogen Energy*, 2014, **39**, 6328–6334.
22 T. P. Huang, Q. Gao, D. Liu, S. N. Xu, C. B. Guo, J. J. Zou and C. D. Wei, *Int. J. Hydrogen Energy*, 2015, **40**, 2354–2362.
23 W. J. Yang, T. Y. Zhang, J. H. Zhou, W. Shi, J. Z. Liu and K. F. Cen, *Energy*, 2015, **88**, 537–543.

24 B. Alinejad and K. Mahmoodi, *Int. J. Hydrogen Energy*, 2009, **34**, 7934–7938.

25 E. Czech and T. Troczynski, *Int. J. Hydrogen Energy*, 2010, **35**, 1029–1037.

26 P. Dupiano, D. Stamatis and E. L. Dreizin, *Int. J. Hydrogen Energy*, 2011, **36**, 4781–4791.

27 S. Liu, M. Q. Fan, C. Wang, Y. X. Huang, D. Chen, L. Q. Bai, *et al.*, *Int. J. Hydrogen Energy*, 2012, **37**, 1014–1020.

28 S. S. Razavi-Tousi and J. A. Szpunar, *Metall. Mater. Trans. E*, 2014, **1**, 247–256.

29 S. S. Razavi-Tousi and J. A. Szpunar, *Electrochim. Acta*, 2014, **127**, 95–105.

30 Y. A. Liu, X. H. Wang, H. Z. Liu, Z. H. Dong, S. Q. Li, H. W. Ge and M. Yan, *Energy*, 2014, **72**, 421–426.

31 Y. A. Liu, X. H. Wang, H. Z. Liu, Z. H. Dong, S. Q. Li, H. W. Ge and M. Yan, *Energy*, 2015, **84**, 714–721.

32 Y. A. Liu, X. H. Wang, H. Z. Liu, Z. H. Dong, S. Q. Li, H. W. Ge and M. Yan, *RSC Adv.*, 2015, **5**, 60460–60466.

33 Y. A. Liu, X. H. Wang, H. Z. Liu, Z. H. Dong, S. Q. Li, H. W. Ge and M. Yan, *Energy*, 2015, **89**, 907–913.

34 Z. Y. Deng, Y. F. Liu, Y. Tanaka, J. H. Ye and Y. Sakka, *J. Am. Ceram. Soc.*, 2005, **88**, 977–979.

35 Z. Y. Deng, Y. B. Tang, L. L. Zhu, Y. Sakka and J. H. Ye, *Int. J. Hydrogen Energy*, 2010, **35**, 9561–9568.

36 Z. Y. Deng, W. H. Liu, W. Z. Gai, Y. Sakka, J. H. Ye and Z. W. Ou, *J. Am. Ceram. Soc.*, 2010, **93**, 2534–2536.

37 W. H. Liu, W. Z. Gai, Z. Y. Deng and J. W. Tang, *J. Am. Ceram. Soc.*, 2012, **95**, 1193–1196.

38 C. S. Fang, W. Z. Gai and Z. Y. Deng, *J. Am. Ceram. Soc.*, 2014, **97**, 44–47.

39 W. Z. Gai, Y. Shi, Z. Y. Deng and J. G. Zhou, *Int. J. Hydrogen Energy*, 2015, **40**, 12057–12062.

40 H. T. Teng, T. Y. Lee, Y. K. Chen, H. W. Wang and G. Z. Cao, *J. Power Sources*, 2012, **219**, 16–21.

41 W. Z. Gai, C. S. Fang and Z. Y. Deng, *Int. J. Energy Res.*, 2014, **38**, 918–925.

42 Y. Yang, W. Z. Gai, Z. Y. Deng and J. G. Zhou, *Int. J. Hydrogen Energy*, 2014, **39**, 18734–18742.

43 H. X. Meng, N. Wang, Y. M. Dong, Z. L. Jia, L. J. Gao and Y. J. Chai, *J. Power Sources*, 2014, **268**, 550–556.

44 N. Wang, H. X. Meng, Y. M. Dong, Z. L. Jia, L. J. Gao and Y. J. Chai, *Int. J. Hydrogen Energy*, 2014, **39**, 16936–16943.

45 Y. H. Lu and H. T. Chen, *Phys. Chem. Chem. Phys.*, 2015, **17**, 6834–6843.

46 H. W. Wang and M. S. Chin, *Int. J. Chem. Eng. Appl.*, 2015, **6**, 146–151.

47 W. Z. Gai, W. H. Liu, Z. Y. Deng and J. G. Zhou, *Int. J. Hydrogen Energy*, 2012, **37**, 13132–13140.

48 T. C. Li, S. Kheifets, D. Medellin and M. G. Raizen, *Science*, 2010, **328**, 1673–1675.

49 J. Y. Mo, A. Simha, S. Kheifets and M. G. Raizen, *Opt. Express*, 2015, **23**, 1888–1893.

50 Y. H. Qin, *Thermodynamics*, Higher Education Press, Beijing, 2008.

51 Z. Y. Deng, J. M. F. Ferreira, Y. Tanaka and Y. Isoda, *Acta Mater.*, 2007, **55**, 3663–3669.